

The influence of the inter-particle sliding, rolling and torsion resistance on the skew-symmetric stress of sheared granular materials

Noor Lammerts van Bueren^{1,*}, Carlijn Tempelaars^{1,*}, Stefan Luding^{1,**}, and Max Winkelmann^{1,2}

¹University of Twente, Enschede, The Netherlands

²School of Engineering, The University of Edinburgh, UK

Abstract. Granular materials are made of discrete particles that interact with each other through their contacts (forces and torques). On the example of a particle simulation of a Cartesian (planar) split-bottom shear cell, we show the effect of microscopic resistance contact parameters between spherical particles on macroscopic continuum fields. Our results show that rolling friction has the strongest effect on the non-classical micropolar skew-symmetric stress. This skew-symmetric stress peaks in the same area as the shear band, and remains finite outside of it for vanishing shear rate. Its magnitude shows an increasing correlation with increasing shear band width. Torsion resistance has a similar, but smaller influence, whereas the correlation of sliding resistance only is almost negligible.

1 Introduction

Granular materials consist of discrete particles which interact with each other through their frictional contacts. Any change of properties at grain level affects the response of the material on the macro scale.

It has been shown that torques at micro scale can lead to a macroscopic asymmetric stress tensor [1, 2]. While micropolar modelling of granular materials has picked up interest in recent years [3], the impact of different microscopic contact resistances on the macroscopic skew-symmetric stress has not been studied much.

A Cartesian (planar) split-bottom shear cell is modeled with the Discrete Element Method (DEM). Through discrete-to-continuum (D2C) upscaling methods, the discrete particle data such as particle mass, particle velocity, and contact force can be mapped onto classical continuous fields like density, velocity, and stress [2, 4]. From those fields, the velocity gradient, skew-symmetric stress tensor, and the macro shear band width can be determined. Their relations to the grain level sliding, rolling, and torsion resistances, are then studied to understand the influence of microscopic contact quantities on non-classic macroscopic continuum fields.

2 Method

The simulations of a Cartesian (planar) split-bottom shear cell [5] are performed with the open-source DEM software MercuryDPM [6]. The obtained discrete data is time-averaged and spatially coarse-grained towards smooth

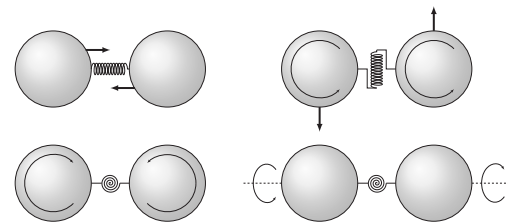


Figure 1. Spring-dashpot model for all degrees of freedom: normal resistance (top left), sliding resistance (top right), rolling resistance (bottom left) and torsion resistance (bottom right) (adapted from [9]).

continuous fields to analyse the skew-symmetric stress and the shear band.

2.1 Particle mechanics and simulation set-up

The interactions between particles are modeled as elastic-plastic spring-dashpots using the discrete element method (DEM) [7, 8]. Fig. 1 shows the different degrees of freedom between two particles and their responding spring-dashpot model where the linear and circular arrows represent forces and torques [9]. The problem reduces to solving Newton's equations of translational and rotational motion, including interaction forces, gravity and possible external loads. Tangential forces, sliding, rolling, and torsion resistances lead to torques [8]. This research contains a parameter study on the rolling μ_r , torsion μ_t and sliding resistance μ_s coefficients.

Fig. 2 shows a schematic of the Cartesian (planar) split-bottom shear cell. The dimensionless interaction parameters are chosen similarly as in [4, 10] to simulate glass

*Contributed equally

**e-mail: s.luding@utwente.nl

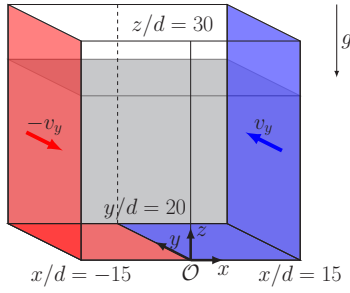


Figure 2. Schematic of the split bottom shear cell where both sides and ground surfaces move with the same velocity v_y in opposite directions. Gravity acts in the negative z -direction.

beads with an average diameter of $d = 1$ and a mass of $m = 1$ (density $\rho = 6/\pi$). The time scale is set via the gravitational acceleration $g = 1$, and thus the contact time is $t_c = 0.05$. A slight polydispersity is applied to avoid crystallisation, with uniform particle size distribution in the range of $d \in [0.88, 1.10]$. The normal contact stiffness is 2000 and other contact stiffnesses are chosen such that the time steps for each degree of freedom are the same, namely $k_s = 2/7k_n$ and $k_r = k_t = 2/5k_n$. The damping coefficients are chosen as $\gamma_n = \gamma_s = \gamma_r = \gamma_t = 2.5$, which results a normal coefficient of restitution $e_n = 0.88$ [4, 10].

Periodic boundary conditions in the depth of the cell (y -direction) are applied. The walls are made out of fixed particles of the same material to avoid slip and are moving in opposite y -directions with a velocity $v_y = 0.0125$ to shear the material, creating a steady-state.

Before studying the influence of rolling and torsion resistance, an initial campaign is run with varying sliding resistances as reference (campaign A). Afterwards, μ_r and μ_t and combinations thereof are varied (campaigns B - F), see Tab. 1. Resistances larger than 10 do not have any further significant impact. The effect of the inter-particle resistance is generally already saturated around a value of $\mu < 1$ [11]. The sliding resistance is kept at $\mu_s = \mu_n = 0.5$ throughout the campaigns B - F. Subscripts are introduced to refer to the specific cases of no friction (*e.g.*, A_0), friction of 0.5 (*e.g.*, $A_{0.5}$) and high friction (*e.g.*, A_1).

Table 1. The resistance parameter configurations for all simulation campaigns. For a varying resistance, it states $[0, 1]$, indicating a range from 0 to 1 with steps of 0.1.

Campaign	μ_s	μ_r	μ_t
A	[0, 1]	0	0
B	0.5	[0, 1]	0
C	0.5	0	[0, 1]
D	0.5	[0, 1]	10
E	0.5	10	[0, 1]
F	0.5	[0, 1]	$\mu_t = \mu_r$

2.2 Analysis of continuous fields

The discrete data is averaged in time and space to avoid discrete fluctuations and to obtain smooth continuous

fields [2, 4] with an averaging length of $w/d = 1$ for the standard deviation of a Gaussian kernel. Due to the periodic boundary conditions, the data can be averaged over y . The coarse grained velocity field, \mathbf{v} , is defined as the momentum divided by density,

$$\mathbf{v}(\mathbf{r}, t) \equiv \sum_{\alpha} m_{\alpha} \mathbf{v}_{\alpha} \phi(\mathbf{r} - \mathbf{r}_{\alpha}) \cdot \left(\sum_{\alpha} m_{\alpha} \phi(\mathbf{r} - \mathbf{r}_{\alpha}) \right)^{-1}, \quad (1)$$

with m_{α} being the mass, \mathbf{v}_{α} the velocity and \mathbf{r}_{α} the location of particle α , \mathbf{r} the point from where the velocity is assessed and ϕ the smoothing kernel. Its gradient, the strain rate, can be used to define the shear band, which is a relatively small area in which the shear concentrates [12] via

$$\widehat{\partial_x v_y}(x, z) = \frac{\partial_x v_y(x, z)}{(\partial_x v_y)_{\max, x}(z)}. \quad (2)$$

A shear band is identified if the normalised shear rate is above $\widehat{\partial_x v_y} > 0.6$ [12]. Since the width of the shear band, S/d , has small variances over the height, its average is taken. The exact choice of the averaging window has only a minor influence as long as it is not too close to the top and the bottom and is therefore chosen as $z/d \in [5, 20]$.

The stress tensor can be decomposed into a kinetic and a contact stress, but only the latter is contributing to the skew-symmetric stress [2, 4] via

$$\sigma_{[ij]} = \frac{1}{2} \sum_{\alpha\beta} \epsilon_{ijk} [\mathbf{r}_{\alpha\beta} \times \mathbf{f}_{\alpha\beta}]_k \times \int_0^1 \phi(\mathbf{r} - \mathbf{r}_{\alpha} + s\mathbf{r}_{\alpha\beta}) ds, \quad (3)$$

where $\mathbf{f}_{\alpha\beta}$ is the contact force between particles α and β , $\mathbf{r}_{\alpha\beta}$ the branch vector from the centre of mass of particle α to the centre of mass of particle β , and ϵ_{ijk} the Levi-Civita symbol. If only normal forces are present, the stress is symmetric in equilibrium within the limitation of spherical particles. Sliding, rolling and torsion resistance result in torques that have to be balanced by the skew-symmetric stress.

The skew-symmetric stress tensor can be quantified using its second invariant K_2 which corresponds to the deviatoric invariant J_2 . Diagonal entries of a skew-symmetric tensor vanish, such that K_2 is defined as

$$K_2 = \sigma_{[12]}^2 + \sigma_{[23]}^2 + \sigma_{[13]}^2. \quad (4)$$

3 Results and discussion

For each simulation campaign from Tab. 1, the shear band is defined and the skew-symmetric stress is calculated using the previously described methods, and then discussed.

3.1 Shear band width

Shear bands are forming in the center of the shear cell around $x/d = 0$. Exemplary for all other cases, Fig. 3 shows the full shear band for a sliding friction of $\mu_s = 0.5$, and no rolling and torsion friction, $\mu_r = \mu_t = 0$.

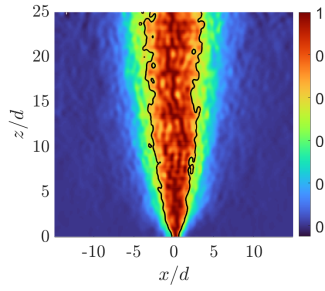


Figure 3. Normalised velocity gradient, $\widehat{\partial_x v_y}(x, z)$, with $\mu_s = 0.5, \mu_r = \mu_t = 0$. The black contour indicates the boundaries of the shear band using a threshold $\widehat{\partial_x v_y} = 0.6$ as cutoff.

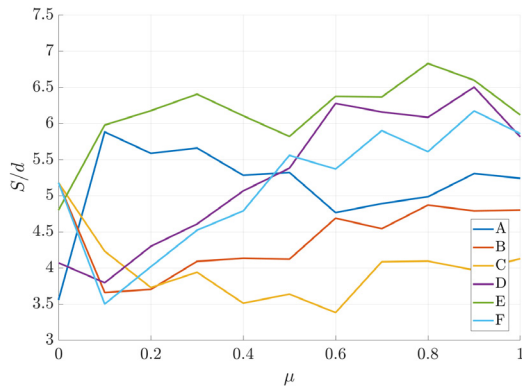


Figure 4. Dependence of shear band width, S/d , on resistance for the six different simulation campaigns. The shear band width is the average band width over a range of $5 \leq z/d \leq 20$ per x/d .

The shear band width S/d , as defined in Sect. 2.2, is plotted over resistance for all simulation campaigns in Fig. 4. The width is the smallest when no friction is present at all (left end of blue curve). Activating sliding resistance causes a sudden jump in width but directly stabilizes and even slowly decreases when the sliding resistance gets higher. Rolling resistance results in a slight increase of the shear band width (red curve, B), while torsion resistance has little effect on it (yellow curve, C).

When comparing the purple (D) and green (E) curves it is clear that the effect of rolling resistance on the shear band width is more dominant than the effect of torsion resistance. Furthermore, a high rolling resistance causes particles to interlock which results in a smoother velocity gradient. This gives a wider shear band and the effect can be seen in the purple (D), green (E) and light blue (F) curves.

3.2 Skew-symmetric stress

The average of skew-symmetric stress, $\sqrt{K_2}$, over pressure within the range $z \in [5, 20]$ is shown in Fig. 5 for sliding friction only ($A_{0.5}$, blue curve), high rolling friction (B_1 , red curve), and high torsion (C_1 , yellow curve). It is low and constant along the width of the cell if both rolling and torsion resistance are deactivated (blue curve). However, it has a peak inside the shear band around the center of the cell when rolling and/or torsion resistance are included.

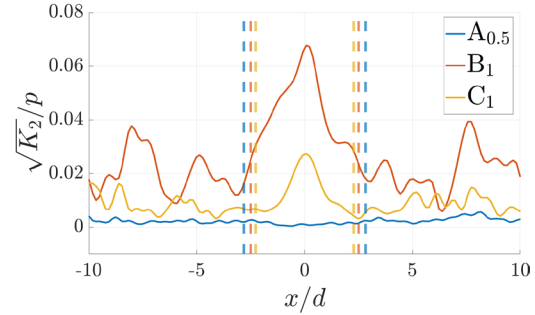


Figure 5. Influence of rolling and torsion friction of skew-symmetric stress scaled by pressure, plotted over the width of the shear cell. The dashed lines indicate the location of the corresponding shear bands, using $\widehat{\partial_x v_x} = 0.6$.

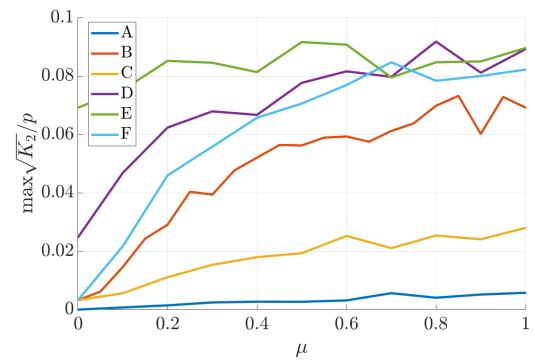


Figure 6. Influence of friction on the maximum skew-symmetric stress for the six simulation campaigns.

Rolling resistance has a more significant effect, where the skew-symmetric stress magnitude reaches approximately 7% of the pressure, whereas it only gets up to around 3% for high torsion resistance. In the case of varying rolling resistance, the skew-symmetric stress appears finite outside the shear band as well. However, its major peak is located inside the shear band.

The dependence of the peak of the skew-symmetric stress on friction is visualized in Fig. 6. Having no resistance (blue curve at $\mu_s = \mu_r = \mu_t = 0$) gives no skew-symmetric stress. Exclusively including sliding resistance causes a small increase (blue curve, A), but below 0.5%. The effects of rolling resistance (red curve) and torsion resistance (yellow curve, C) are much stronger. When rolling resistance is kept constant at a high value of $\mu_r = 10$ and the torsion friction is varied, the effect seems to be saturated (green curve, E). If the torsion friction is kept high and the rolling friction is varied, the skew-symmetric stress is increasing (purple curve, D). This shows that the effect of the rolling resistance is dominant.

All the cases which end with both $\mu_r \geq 1$ and $\mu_t \geq 1$ (green, purple and light blue) lead to a skew-symmetric stress of above 8% of the total pressure, which seems to be the limit for this shear cell configuration.

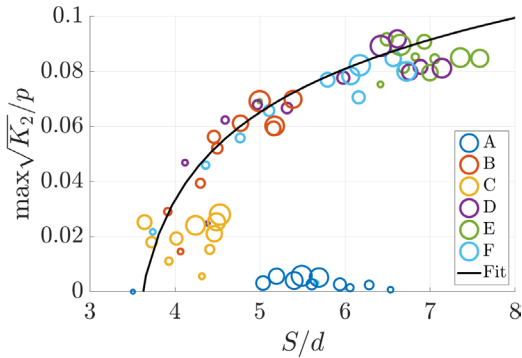


Figure 7. Relation between the maximum skew-symmetric stress and the shear band width. The dot size indicates the magnitude of the varying resistance.

3.3 Relation between shear band width and skew-symmetric stress

Similar trends can be found for the shear band width, see Fig. 4, and the peak skew-symmetric stress, see Fig. 6: both quantities seem to increase with higher resistances, especially for rolling resistance.

The skew-symmetric stress peak is plotted against the shear band width in Fig. 7. When varying rolling resistance (especially red, purple, and light blue circles), the data points are widely distributed. In contrast the data is clustered when the torsion resistance is varied (yellow and green circles) showing again that rolling resistance has a larger influence. All data points are collapsing if the sliding simulation campaign is not taken into account. The peak skew-symmetric stress is increasing with increasing shear band width, following the trend of a master curve of the shape $\frac{\max \sqrt{K_2}}{p} \approx \alpha \left(\frac{S}{d} - \frac{S_0}{d} \right)^\beta + \zeta$ with $\alpha = 48.48$, $\beta = 0.0006689$, $\zeta = -48.43$, and $\frac{S_0}{d} = 3.4$.

4 Conclusion

The contact sliding, rolling, and torsion resistances certainly have an impact on the bulk properties of granular matter. Including only normal forces leads to classical stress behaviour while adding sliding resistance gives very little skew-symmetry. With either rolling or torsion resistance, skew-symmetric stress emerges throughout the cell with a peak in the center of the shear band. Rolling resistance has a more significant impact compared to torsion resistance. For both high rolling and torsion resistance, the skew-symmetric stress reaches a non-negligible magnitude of around 7% of the total hydrostatic pressure.

An increase in resistance leads to a wider shear band and a higher magnitude of skew-symmetric stress. While a stronger skew-symmetric stress goes along with a wider shear band, this does not hold vice-versa: The shear band always exists with very small or even without skew-symmetric stress as shown for cases with sliding resistance only. Particle shape might promote the observed effects even further since branch vectors and normal forces do not necessarily align which could lead to additional skew-symmetric stresses [13]. In addition, the effect of softness

and consequently enhanced contact areas and torques is a possible subject for future research.

References

- [1] J.P. Bardet, I. Vardoulakis, Asymmetry of stress in granular media, *International Journal of Solids and Structures* **38** (2001). [10.1016/S0020-7683\(00\)00021-4](https://doi.org/10.1016/S0020-7683(00)00021-4)
- [2] I. Goldhirsch, Stress, stress asymmetry and couple stress: from discrete particles to continuous fields, *Granular Matter* **12**, 239 (2010). [10.1007/s10035-010-0181-z](https://doi.org/10.1007/s10035-010-0181-z)
- [3] J. Tian, Y. Lai, E. Liu, C. He, A thermodynamics-based micro-macro elastoplastic micropolar continuum model for granular materials, *Computers and Geotechnics* **162**, 105653 (2023). [10.1016/j.compgeo.2023.105653](https://doi.org/10.1016/j.compgeo.2023.105653)
- [4] T. Weinhart, R. Hartkamp, A.R. Thornton, S. Luding, Coarse-grained local and objective continuum description of three-dimensional granular flows down an inclined surface, *Physics of Fluids* **25** (2013). [10.1063/1.4812809](https://doi.org/10.1063/1.4812809)
- [5] S. Roy, S. Luding, W. den Otter, A. Thornton, T. Weinhart, Drift-diffusive liquid migration in partly saturated sheared granular media, *Journal of Fluid Mechanics* **915** (2021). [10.1017/jfm.2021.30](https://doi.org/10.1017/jfm.2021.30)
- [6] T. Weinhart, L. Orefice, M. Post, M.P. van Schrojenstein Lantman, I.F. Denissen, D.R. Tunuguntla, J. Tsang, H. Cheng, M.Y. Shaheen, H. Shi et al., Fast, flexible particle simulations — An introduction to MercuryDPM, *Computer Physics Communications* **249** (2020), <https://www.mercurydpm.org>. <https://doi.org/10.1016/j.cpc.2019.107129>
- [7] P.A. Cundall, O.D.L. Strack, A discrete numerical model for granular assemblies, *Géotechnique* **29**, 47 (1979). [10.1680/geot.1979.29.1.47](https://doi.org/10.1680/geot.1979.29.1.47)
- [8] S. Luding, Cohesive, frictional powders: contact models for tension, *Granular Matter* **10**, 235 (2008). [10.1007/s10035-008-0099-x](https://doi.org/10.1007/s10035-008-0099-x)
- [9] A. Merkel, S. Luding, Enhanced micropolar model for wave propagation in ordered granular materials, *International Journal of Solids and Structures* **106-107**, 91 (2017). [10.1016/j.ijsolstr.2016.11.029](https://doi.org/10.1016/j.ijsolstr.2016.11.029)
- [10] L.E. Silbert, D. Ertas, G.S. Grest, T.C. Halsey, D. Levine, S.J. Plimpton, Granular flow down an inclined plane: Bagnold scaling and rheology, *Physical Review E* **64** (2001). [10.1103/PhysRevE.64.051302](https://doi.org/10.1103/PhysRevE.64.051302)
- [11] A. Singh, V. Magnanimo, S. Luding, in *Numerical Methods in Geotechnical Engineering*, edited by M. Hicks, R. Brinkgreve, A. Rohe (CRC Press, 2014), pp. 409–414
- [12] T. Weinhart, C. Labra, S. Luding, J.Y. Ooi, Influence of coarse-graining parameters on the analysis of DEM simulations of silo flow, *Powder Technology* **293**, 138 (2016). [10.1016/j.powtec.2015.11.052](https://doi.org/10.1016/j.powtec.2015.11.052)
- [13] M. Winkelmann, V. Magnanimo, S.A. Papanicolaou, S. Luding, Shape-induced micropolar effects in granular media (2025), in preparation.